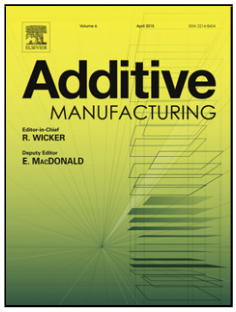

Title: Tensile properties and failure behavior of chopped and continuous carbon fiber composites produced by Additive Manufacturing

Authors: Juan Naranjo Lozada, Horacio Ahuett-Garza, Pedro Orta Castañón, Wilco M.H. Verbeeten, Daniel Sáiz González

PII: S2214-8604(18)30604-3
DOI: https://doi.org/10.1016/j.addma.2018.12.020
Reference: ADDMA 619

To appear in:

Received date: 10 August 2018
Revised date: 22 December 2018
Accepted date: 22 December 2018

Please cite this article as: Lozada JN, Ahuett-Garza H, Castañón PO, Verbeeten WMH, González DS, Tensile properties and failure behavior of chopped and continuous carbon fiber composites produced by Additive Manufacturing, *Additive Manufacturing* (2019), https://doi.org/10.1016/j.addma.2018.12.020

Tensile properties and failure behavior of chopped and continuous carbon fiber composites produced by Additive Manufacturing

[1]Juan Naranjo Lozada, [1]Horacio Ahuett-Garza, [1]Pedro Orta Castañón, [2]Wilco M.H. Verbeeten, [3]Daniel Sáiz González

[1] Escuela de Ingenieria y Ciencias, Tecnologico de Monterrey
Ave. Eugenio Garza Sada 2501, Monterrey, N.L., México, 64849
[2] Structural Integrity Research Group, Universidad de Burgos
Avenida Cantabria s/n, E-09006 Burgos, Spain
[3] Escuela Politécnica Superior, Universidad de Burgos
Avenida Cantabria s/n, E-09006 Burgos, Spain

Corresponding author: Horacio Ahuett-Garza
Email: horacio.ahuett@itesm.mx

Abstract

The use of additive manufacturing (AM) is rapidly expanding in many industries mostly because of the flexibility to manufacture complex geometries. Recently, a family of technologies that produce fiber reinforced components has been introduced, widening the options available to designers. AM fiber reinforced composites are characterized by the fact that process related parameters such as the amount of reinforcement fiber, or printing architecture, significantly affect the tensile properties of final parts. To find optimal structures using new AM technologies, guidelines for the design of 3D printed composite parts are needed. This paper presents an evaluation of the effects that different geometric parameters have on the tensile properties of 3D printed composites manufactured by fused filament fabrication (FFF) out of continuous and chopped carbon fiber reinforcement. Parameters such as infill density and infill patterns of chopped composite material, as well as fiber volume fraction and printing architecture of continuous fiber reinforcement (CFR) composites are varied. The effect of the location of the initial deposit point of reinforcement fibers on the tensile properties of the test specimens is studied. Also, the effect that the fiber deposition pattern has on tensile performance is quantified. Considering the geometric parameters that were studied, a variation of the Rule of Mixtures (ROM) that provides a way to estimate the elastic modulus of a 3D printed composite is proposed. Findings may be used by designers to define the best construction parameters for 3D printed composite parts.

Keywords:

Mechanical properties; Additive manufacturing; Continuous fiber composite; Chopped composites Carbon fiber; Rule of Mixtures.

Nomenclature

E_{matrix}	Matrix elastic modulus
E_{fiber},	Fiber elastic modulus

$\boldsymbol{\varphi_{fiber}}$	Fiber volume fraction
$\boldsymbol{\varphi_{matrix}}$	Matrix volume fraction
$\mathbf{V}_i$	Region volumes
$\mathbf{V}_{composite}$	Overall volume
$\boldsymbol{E_{predicted}}$	Predicted elastic modulus
$\mathbf{W}_{wall}$	Wall strand width
$\mathbf{W}$	Overall width
$\mathbf{W}_{fiber}$	Fiber strand width
$\mathbf{T}$	Overall thickness
$\mathbf{T}_{layer}$	Layer thickness
$\mathbf{H}$	Tensile length
$\mathbf{N}$	Total number of layers
$\mathbf{N}_{walls}$	Number of wall rings
$\mathbf{N}_{floor}$	Number of floor layers
$\mathbf{N}_{roof}$	Number of roof layers
$\mathbf{N}_{fiber}$	Number of reinforced layers
$\mathbf{R}_{fiber}$	Number of Reinforced rings

1. Introduction

Rapid prototyping was introduced in the decade of 1980. Since then, various additive manufacturing processes have been developed. In the early years, these technologies focused on prototyping. However, during the last 20 years, they have evolved into the additive manufacturing technologies known today, that are oriented to the production of functional parts.

Among all the AM process, the most widely used 3D printing methods for processing polymer composites are selective laser sintering (SLS) and fused deposition modeling (FDM), also known as fused filament fabrication (FFF). In comparison to SLS, the FFF process has the advantages of low input energy and material cost, minimum waste, and consistent prototype accuracy [1]. Additionally, FFF has other advantages such as no need for chemical post-processing, and less expensive machines and materials, which result in a cost-effective process [2]. On the other hand, FFF parts have limited mechanical properties. To overcome these limitations new approaches to produce 3D printed composites are being proposed, for example, different techniques of particle reinforced composites, short-fiber reinforced composites and nano-composites were summarized in [3] by Wang et al.

Recently, a variation of FFF [4] that produces continuous fiber reinforced (CFR) components was introduced. In this process, reinforced fibers of different types are combined with conventional polymers to produce reinforced parts. The method uses independent nozzles to process reinforced materials such as carbon fiber, fiberglass, or Kevlar, with a conventional polymer that serves as a matrix. Parts produced by this process have shown properties that are comparable to aluminum, which has raised much interest for their potential use in engineering applications [5] [6].

In addition to the process parameters, composite parts manufactured by AM technologies are affected by how the fibers are incorporated into the polymer matrix, geometric parameters (such as infill density and infill patterns), and the amount and arrangement of the fibers. While there is a vast amount of knowledge and experience for the design of parts made out of composite materials using conventional

production methods [7], designers of parts that use the new AM technologies need guidelines that are compatible with the new processes, and that facilitate the introduction of AM parts in engineering applications. As a consequence, there is a growing interest in establishing process parameters (speed, temperatures, etc.) that improve part properties, and reduce the fabrication time as well as the cost of FFF parts.

Most of the commercial AM machines and their software limit the changes that users can make to process parameters such as deposition speed or material temperature. In contrast, non-commercial slicing software used to convert the CAD designs into printing layers offer several geometric parameter control options, such as infill density, infill pattern, layers thickness, etc. Characterizing and understanding the effects that the printing parameters have on the final properties of the 3D printed composites parts can play an important role in the capacity of this type of parts to be used in engineering applications.

According to Prüß, H. et al. [8] there are several different possibilities for fiber integration into the part. In particular for FFF composites, and considering the time and location of the fiber incorporating process, there are three methods of fiber implementation that seem more viable:

- Type 1, incorporation of the fiber before the printing process, that is, the filament itself is a composite (Figure 1a)
- Type 2, incorporating it in the print head, meaning, two materials are combined when they pass through the extruder (Figure 1b)
- Type 3, incorporating it on the component, thus requiring two or more independent extruders, each one with an independent nozzle (Figure 1c)

This classification is relevant because the properties of the part depend not only on the amount, often measured in terms of the volume fraction of the reinforcing fiber, but also on the manner in which the fibers are integrated into the matrix material.

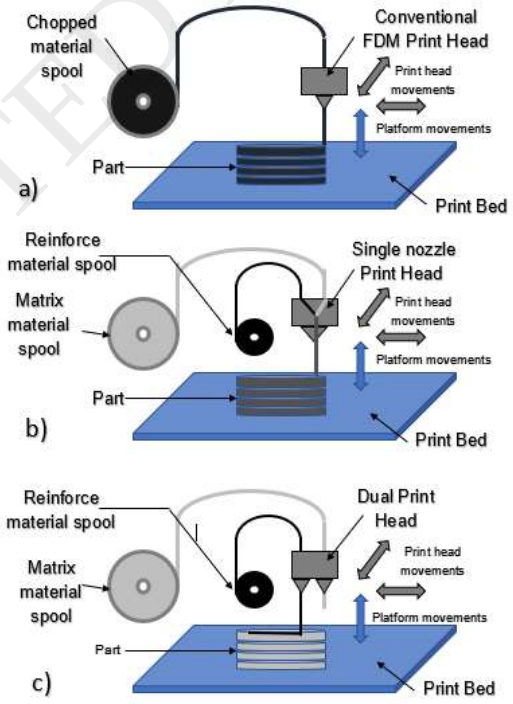

Figure 1. Fiber reinforced FFF types a) Type 1 b) Type 2. c) Type 3.

Currently, equipment for Type 1 and Type 3 methods is commercially available. In contrast, Type 2 method equipment is still at the development stage. In particular, the head mechanism that incorporates the fiber into the polymer matrix must be designed and tested for each application, depending on the fiber and matrix polymer characteristics.

In this work, a machine that is capable of Type 1 and Type 3 processes is used to explore the relationship of process conditions with part properties. The first part of this study focuses on the evaluation of the mechanical performance of Type 1 FFF composites. The effects of Infill Density and Infill Patterns in Onyx samples were compared with Nylon samples with the same geometric parameters. In this context, Infill Patterns refers to the geometric shapes repeated on the inside of the part, while the Infill Density is the amount of polymer material (Onyx or Nylon) deposited inside the part. Other geometric variables, such as the number of roof / floor layers, and width of walls (refered to as shell) were kept constant for all the tests.

The second part of this work analyzes the influence of fiber volume fraction (VF) and fiber placement arrangement on the mechanical performance of Type 3 FFF parts. Analysis of the results from these tests suggested that the initial point of application of the reinforcement fiber affects the tensile properties of the specimen. For this reason, an exploratory study about the effect that the point of initial application of the reinforcing fiber has on part properties was also conducted.

The article is organized as follows. Section 2 presents a state of the art review for fiber reinforced AM technologies. Section 3 presents the characteristics of the materials tested, the geometric parameters evaluated, and the fabrication and characterization equipment. Section 4 shows the results and discussion for volume fraction calculations. The tensile properties results, as well as mesostructure and fatigue mechanism analysis for specimens produced by Type 1 and Type 3 processes are presented in Section 4. Section 5 proposes a complementary method based on the Rule of Mixtures to predict the elastic modulus of the CFR specimens, while in Section 6 the effect of the start point of reinforcement on mechanical properties for CFR composites is analyzed. Finally, Section 7 presents some implications for part design, and Section 8 summarizes the conclusions and future work.

2. Literature Review

Ning et al. [1] reported the fabrication of Type 1 CFR specimens using an FDM machine (Creatr, Leapfrog Co.) and a composite filament (FilaBot Co.) with a diameter of 1.75 mm which contained 5 % (weight percentage) chopped carbon fiber and acrylonitrile-butadiene-styrene (ABS) thermoplastic matrix. In their work, they evaluated the mechanical properties for different values of four process parameters: nozzle temperature, infill speed, raster angle and layer thickness. Their goal was to find the best parameters to improve the tensile strength of the parts. Stratasys recently introduced FDM Nylon 12CF, a carbon fiber-filled thermoplastic, which contains 35% chopped carbon fiber by weight, characterized by a high flexural strength and stiffness-to-weight ratio [9].

Examples of parts produced by a Type 2 machine were reported by Yang et al. [10] and Tian et al. [11]. They presented a 3D printing equipment with a novel composite extrusion head that can process continuous carbon fiber with ABS and PLA respectively. Also, a novel technique called continuous lattice fabrication (CLF) was proposed by Eichenhofer et al. [12]. The CLF head is comprised of a two-stage, pultrusion-extrusion system. They reported an increase in tensile properties for carbon fiber-reinforced PA12 composites, that can reach tensile strength of 560 MPa and elastic moduli of 83 GPa along the fiber direction. The technique include a softening cycle procedure [13] that attempts to maximize the mechanical

properties of the printed composites by minimizing the residual void content.

Examples of Type 1 and Type 3 machines are presented by Wang et al.[3] in a review for 3D printing polymer composites. Baumann et al. [5] reported that Type 3 machines produce a considerable increase in tensile strength and elastic modulus for different cases of continuous carbon fibers reinforced polymers. This study showed the potential that these processes have to produce functional parts for engineering applications. Other examples of Type 3 processes are presented by Dickson et al. [6], who reported the fabrication of continuous carbon, fiberglass and Kevlar fiber reinforced polymer composites on a Markforged Markone 3D printer. In particular, they evaluated the tensile and flexural properties of test specimens with carbon fiber reinforcement and concluded that these materials could reach tensile strengths of up to 368 MPa, which exceeds the strength of some conventional structural materials, such as Aluminum 6061-T6. They also analyzed the effect of the increase of volume fraction of fiberglass on tensile properties of the material. Melenka et al. [14] presented an evaluation of the tensile properties of 3D printed structures reinforced with Kevlar and propose a method to predict the elastic modulus using compliances matrices. Van der Klift et al. [15] presented an evaluation of tensile properties for two carbon fiber 3D printed specimens and present a prediction of the elastic modulus by the rule of mixtures of composites. Additional investigations for fiber reinforcement during 3D printing have been conducted for medical applications, like those reported by Christ et al. [16]. Also, Turk et al. [17][18] presented a novel manufacturing process to fabricate highly integrated lightweight structures. Other works analyzed the effect of process parameters on final mechanical properties, such as the case of Yang et al.[10] and Spackman et al.[19].

A significant effort has been made to correlate process parameters of new AM technologies with part properties. On the other hand, there are few studies of the effect of fiber geometric patterns on design aspects. Fernandez et al. [20] present an evaluation of infill patterns or infill density in tensile mechanical behavior of ABS parts. Courter et al. [21] conducted a material characterization of ABS specimens to obtain as-built properties including the bead aspect ratio, void ratio, void shape and bonding between beads that were used in finite element (FE) simulation of the FFF process. Their results show that FE simulations capture the interaction between tool path and their impact on the final state of the printed part. Klahn et al. [22] presented some cases for SLS and SLM that showed how the re-design of the part geometry for AM contributed to the success of the product, improving its technological and economic viability.

From the previous discussion, process parameters as well as geometric variables such as infill patterns, infill density, and part shape (void ratio, void shape and bonding between beads) affect the final mechanical properties of 3D printed composites. Much work is still needed to develop product design guideliens that match finished part properties, with materials properties of the feedstock and AM process capabilities, in a way to build Design for Additive Manufacturing capabilities. In particular, this work focused on the evaluation of the effects that fiber arrangement and part geometry have on tensile properties of 3D printed composites, in an effort to help designers produce viable AM applications.

3. Experimental Setup

3.1. Materials and Fabrication Equipment

In this work, three different types of specimens are fabricated and tested.

- Nylon samples printed with a PA6 (Polyamide 6) a copolymer filament produced in the form of a wire
- Samples printed with Onyx, a nylon filament that is strengthened with chopped carbon fibers, and

- CFR composites: nylon filament used as matrix, reinforced with continuous carbon fibers processed using the Type 3 method

Nylon and Onyx filaments are supplied with a diameter of 1.75 mm, while the reinforcing carbon fiber filament is supplied with a diameter of 0.35 mm [23]. The reinforcement material is a filament that may contain up to 1000 individual carbon fibers infused with a sizing agent, as reported in [8]. Fiberglass and Kevlar are also available as reinforcement fibers. Figure 2 shows the different types of specimens printed.

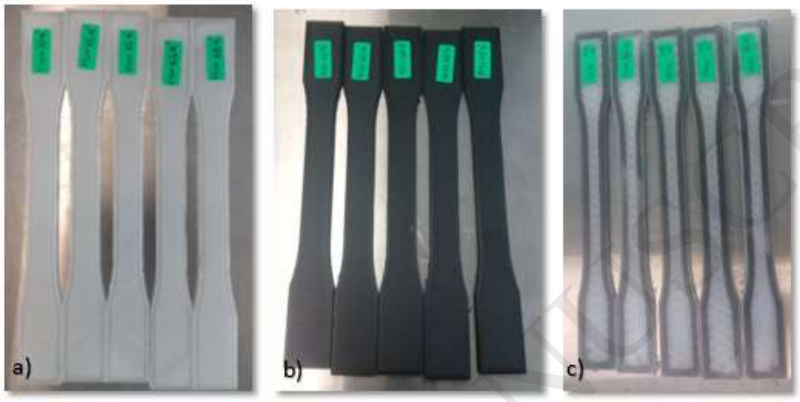

Figure 2. 3D Printed Specimens for a) Nylon b) Onyx and c) CFR composites.

Test specimens were fabricated in accordance with ASTM D638 Standard Test Method for Tensile Properties of Plastic. Section 6.1.3 of this standard recommends that reinforced composites, including highly orthotropic laminates, shall conform to the dimensions of the Type I specimen (1). This geometry was also chosen because it has a larger cross section area. The larger cross-section allows to have more reinforcing material.

A Markforged Marktwo commercial 3D printer machine was used to print all the specimens. The printer has a dual extrusion head that allows the manufacture of CFR composites parts (Type 3 in Figure 1) with different types of fibers: Carbon Fiber, Kevlar, Fiberglass, High-Strength High-Temperature Fiberglass. In this case, the printing process consists of two stages, each of which is performed by a separate print unit in the dual printer head. For this reason the width of nylon matrix strands ($\mathbf{W_{wall}}$) is different from the reinforcing fiber strands ($\mathbf{W_{fiber}}$). The Nylon matrix is printed first, and the reinforcing fiber is deposited in a second stage within the same layer.

The printer can deposit the fiber in a "concentric" pattern that forms annular rings or in a unidirectional pattern called "isotropic" by the manufacturer, that creates continuous reinforced lines in the entire layer. The schematics of the different fiber reinforced patterns is shown in Figure 3. According to Mark [24], Nylon is printed with a hot end temperature of 263◦C onto a non-heated print. The fiber reinforced composite filament is heated in a transverse pressure zone to a temperature higher than the melting temperature of the matrix material. As a result, the matrix material is melted interstitially within the filament. The head applies an ironing force to the melted matrix material.

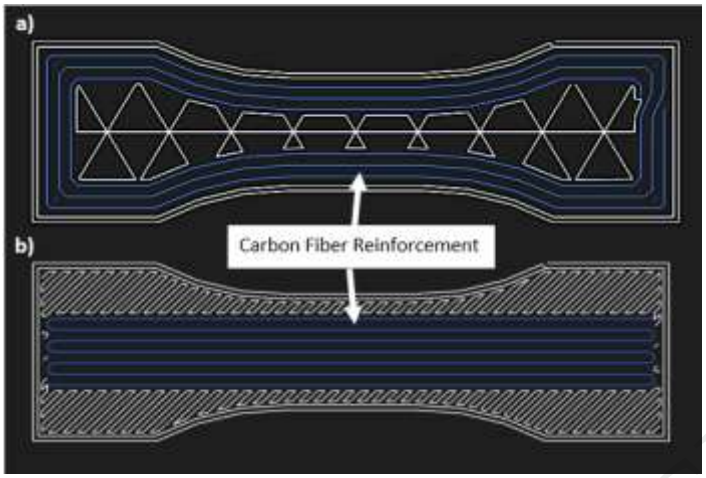

Figure 3. Fiber pattern a) Concentric b) Uni-directional.

This AM machine can also process Type 1 filaments [23]. For Nylon and Onyx, the printing process is similar to a conventional FDM. The dual printing head uses only the plastic nozzle (Figure 1a). The filament is fed through the nozzle which melts, extrudes and deposits the material, layer by layer, in the desired shape, while the moving platform is lowered after each layer is deposited. Table 1 presents details of the geometry used.

Table 1. Overall printing parameters, conforming to a Type I geometry of ASTM D638 Standard.

Sample geometry variable	**Value**	**ASTM D638-14 Type I geometry**
Height (H)-mm	57	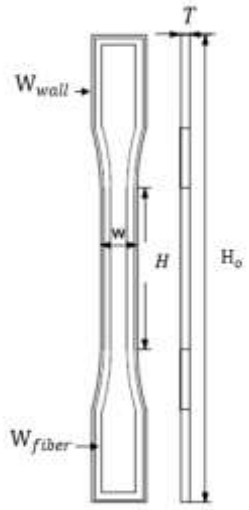
Width (W)-mm	13	
Thickness (T)-mm	3.2	
Layer thickness (T_{layer})-mm	0.125	
Width of Fiber per Ring (W_{fiber})-mm	1	
Width of Wall per Ring (W_{wall})-mm	0.3	
Infill Density (I)-%	10	
Number of Total layers (N)	26	
Number of Floor layers (N_{floor})	4	
Number of Roof layers (N_{roof})	4	
Number of Wall rings (N_{walls})	3	

3.2. Experimental Setups and Test Parameters

Three sets of experiments were conducted, and they are referred to as "Setup" in Table 2. Five specimens for each test of the three different experimental setups were manufactured. The test geometry was created using a computer-aided design (CAD) software package (SolidWorks 2016). The CAD geometry of the specimens was exported as a stereolithography file (STL) and loaded into a cloud slicing software (Eiger). In this software, different parameters were modified for each test of the different experimental setups.

In experimental Setup 1, the matrix materials, the infill patterns, and density parameters were modified to build a full 2^3 factorial experiment with two levels. The following three factors were used:

- Raw Material: Onyx or Nylon
- Infill Density: 10% and 70 %
- Infill Patterns: Rectangular (filaments at 45° with respect to load direction) and Triangular (filaments at 0° or 60° with respect to load direction)

For the continuous carbon fiber reinforcement samples in Setup 2, a "concentric" fiber pattern was selected. For the geometry selected the total number of printing layers is 26. However, the maximum number of reinforced layers is 18, while the maximum number of reinforced concentric rings is 5. The number of concentric rings (R) and the number of layers (L) that contain carbon fiber reinforcement were varied, creating different "printing architectures". In Setup 2, two "printing architectures" with the same fiber content were manufactured. Specimens with only one concentric ring, referred to as 1R in the discussion that follows, and samples with 3 concentric rings referred to as 3R, were printed. The overall printing parameters used to manufacture the test specimens in the different experimental setups are summarized in Table 2.

Table 2. Experimental Setups, Tests, and Main printing parameters.

	Setup 1	**Setup 2**	**Setup 3**
Method of fabrication	Type 1 (Chopped)	Type 3 (CFR)	Type 3 (CFR)
Test description	**Base experiment** 2^3 full factorial design	**Printing Architecture** 1R 6L vs 3R 2L 1R 12L vs 3R 4L 1R 18L vs 3R 6L 3R 18L and 5R 18L	**Fiber Start Point** Outside, Middle, Distributed
Test Parameters	**Levels**		
Infill Density %	10%, 70%	10%	10%
Infill Pattern	Rectangular, Triangular	Triangular	Triangular
Materials	Onyx, Nylon	Nylon Matrix + Carbon Fibers for reinforcement	Nylon Matrix + Carbon Fibers for reinforcement
Number of Specimens	40	40	15

	(5 specimens for each test in 2^3 full factorial design)	(5 specimens for each one of the 8 arrangements)	(5 specimens for each one of the 3 fiber start point test proposed)

For all the specimens in Setups 1 and 2, the starting point for fiber deposition was fixed outside of the tensile area of the specimens. In Setup 3, additional samples for 1R-12L test were manufactured, moving the initial point of the reinforcement fibers to the middle, and uniformly distributed over the tensile area of the specimens. The ASTM D638 Standard does not require the use of tabs in its specimens. However, to reduce the effect of the clamping forces on the specimen, the tabbing guide for composite test specimens [25] was used to attach tab strips in the samples. Tab strips were added using 3M Scotch-Weld DP810 as adhesive and glass fabric / epoxy laminated circuit board as tabbing material.

3.3. Characterization equipment

Tensile tests were performed utilizing three different machines: an Instron 5KN 3365, a SHIMADZU 100 KN and an MTS 810 250KN tension machines. To test 1R-18L and 3R-6L specimens, shown in Table 3, the SHIMADZU machine was used, while 3R-18L and 5R-18L samples were performed on the MTS testing machine due to the high load capacity required to produce a fracture in the specimens. After the tensile tests, the fractured specimens were examined using a Stereo ZEISS optical microscopy for Onyx samples, and SEM EVO MA25 ZEISS microscopy for continuous reinforced samples.

The Elastic modulus (E) in MPa was calculated from the slope of the stress-strain curve with the stresses σ_1 and σ_2 that are measured at strains $\varepsilon_1 = 0.05\%$ and $\varepsilon_2 = 0.25\%$ respectively. Similar to other works [14][26][27], the specimens were held in place using wedge clamps and tested at a crosshead speed of 5 mm/minute as per ASTM D638 standard.

For Nylon and Onyx samples, the tensile strength at yield (in MPa) was estimated. The criteria used was to identify the stress where the parallel line to the elastic modulus line, at 0.02 strain. intersects with the stress-strain curve. For CFR samples the tensile strength at break was used. This was considered to be the maximum stress during the tensile test.

4. Results and Discussion for Setups 1 and 2

4.1. Determination of Fiber Volume Fraction (FVF) by geometric approach

A schematic of the internal structure of the continuous fiber-reinforced 3D printed specimen is shown in Figure 4. Four distinct regions can be distinguished in the test samples: walls region, roof and floor layers, infill layers and reinforced layers. Each region has a different mechanical performance due to the printing toolpath. In the roof and floor layers region the head follows a path in a range of ±45° from the longitudinal axis, while for walls and reinforcement layers the printer toolpath is parallel to the longitudinal axis. Finally, the infill orientation depends on the pattern, Rectangular or Triangular, and the density selected.

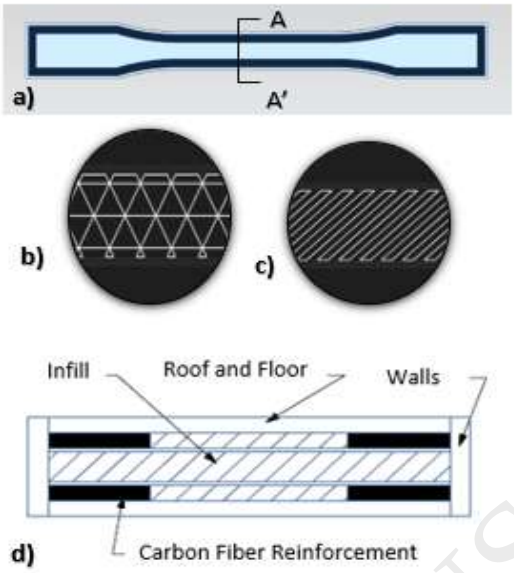

Figure 4. Continuous Carbon Fiber Reinforced specimen a) Top view b) Triangular Infill Pattern c) Rectangular Infill Pattern and d) Cross Section A-A'.

In composites analysis studies, the amount of fiber has been directly correlated with the mechanical properties of the composite, through the fiber volume fraction (FVF), and has been used for stiffness predictions. Methods that can be used to calculate the volume fraction in traditional composite analysis, include the burn-out process [28] [29] or the evaporation process [15] which require the destruction of the specimens by eliminating the matrix material. However, in this study, the fiber volume fraction was calculated using a geometric approach following the procedure reported by Melenka et al. [14].

According to Melenka, the volume of each region of the test specimen can be determined from the geometry of the sample following Equations (1) to (4). The overall composite volume can be calculated using Equation (5). Finally, with Equations (6) the volume fraction of reinforcement fiber can be determined, where φ_{fiber} is the volume fraction of fiber, V_i denotes the volumes of the different regions in the composite, $V_{composite}$ is the overall volume of the specimen, and I is the infill density. Also, N is the total number of layers, while N_{walls}, and N_{floor}/ N_{roof} are the number walls and floor / roof layers selected in the shell of the specimen. Finally, N_{fiber} and R_{fiber}defined the number of layers and concentric rings reinforced with fiber.

$$V_{\text{roof and floor}} = (W - 2 * N_{wall} * W_{wall}) * H * T_{layer} * (N_{floor} + N_{roof}) \quad (1)$$

$$V_{wall} = 2 * N_{wall} * W_{wall} * H * T_{layer} \quad (2)$$

$$V_{infill} = (W - 2 * N_{wall} * W_{wall}) * H * I * T_{layer} * (N - N_{floor} - N_{roof} - N_{fiber}) \quad (3)$$

$$V_{fiber} = 2 * W_{fiber} * N_{fiber} * R_{fiber} * H * T_{layer} \quad (4)$$

$$V_{composite} = W * H * T \quad (5)$$

$$\varphi_{fiber} = \frac{V_{fiber}}{V_{composite}} \quad (6)$$

In this study, the width of fiber strands (Wfiber) and nylon strands (Wwall) were determined with a Stereo ZEISS optical microscope. For calculations, a tensile volume of W=57 mm H= 13mm T= 3.2 mm was considered. The infill density (I) was selected to be 0.1 (10%) and the Layer thickness (T_{layer}) was fixed at 0.125 mm in Eiger. Table 2 summarizes the parameters used in the calculations. An excel template was used to calculate the four region volumes for each printing architecture following Equations (1) to (4). $V_{composite}$ is found using Equation 5, and finally, the fiber volume fraction φ_{fiber} is calculated using Equation (6). Table 3 summarizes the FVF found for all the eight cases in Setup 2. These values were also used for prediction of elastic modulus (Section 5).

Table 3. Volume Fraction calculations for Experimental Setup 2.

Printing Architecture	**Number Concentric Rings (R_{fiber})**	**Number Layers reinforced (N_{fiber})**	**Calculated FVF**
1R 6L	1	6	4%
3R 2L	3	2	4%
1R 12L	1	12	7%
3R 4L	3	4	7%
1R 18L	1	18	11%
3R 6L	3	6	11%
3R 18L	3	18	32 %
5R 18L	5	18	54%

4.2. Experimental Setup 1: Nylon vs Chopped Reinforced samples

4.2.1. Tensile Results

Figures 5 and 6 show a comparison of the effects of infill density and infill pattern for the two types of raw materials, Onyx and Nylon, on the tensile properties of the specimens, for Experimental Setup 1.

Regarding the elastic modulus, tests with Nylon specimens with 10% of infill density and rectangular pattern reported a value of 311.6 MPa (see Appendix 1). Onyx samples with the same parameters displayed an elastic modulus of 581.6 MPa. Same for 70% Rectangular, 10% Triangular and 70% Triangular specimens where the Onyx samples show an increase of 128% (627.3 MPa vs 490.7 MPa), 297% (1064.9 MPa vs 358.4 MPa), and 216% (1293.9 MPa vs 598.9 MPa), respectively, compared to Nylon samples.

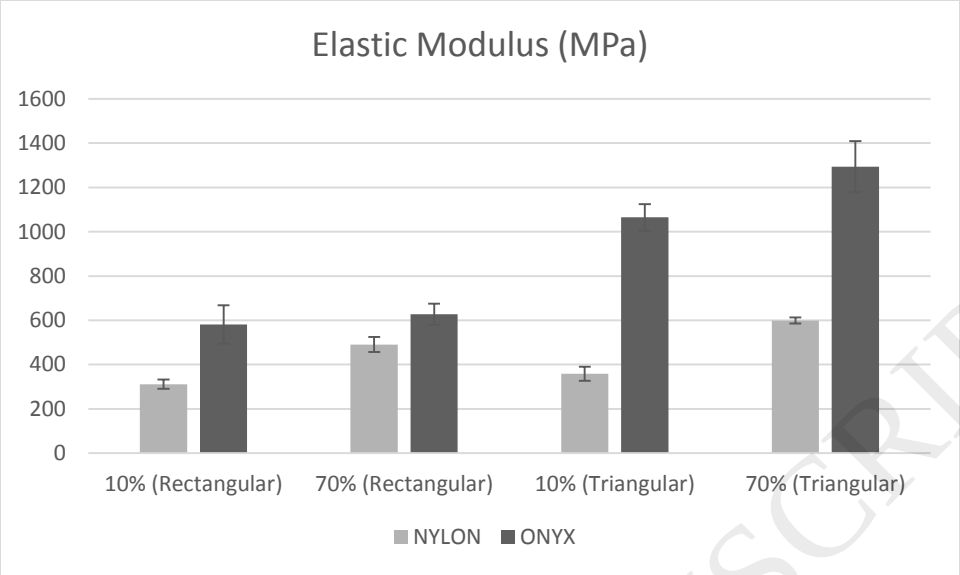

Figure 5. Effect of densities and infill patterns on the Elastic Modulus of Nylon and Onyx samples.

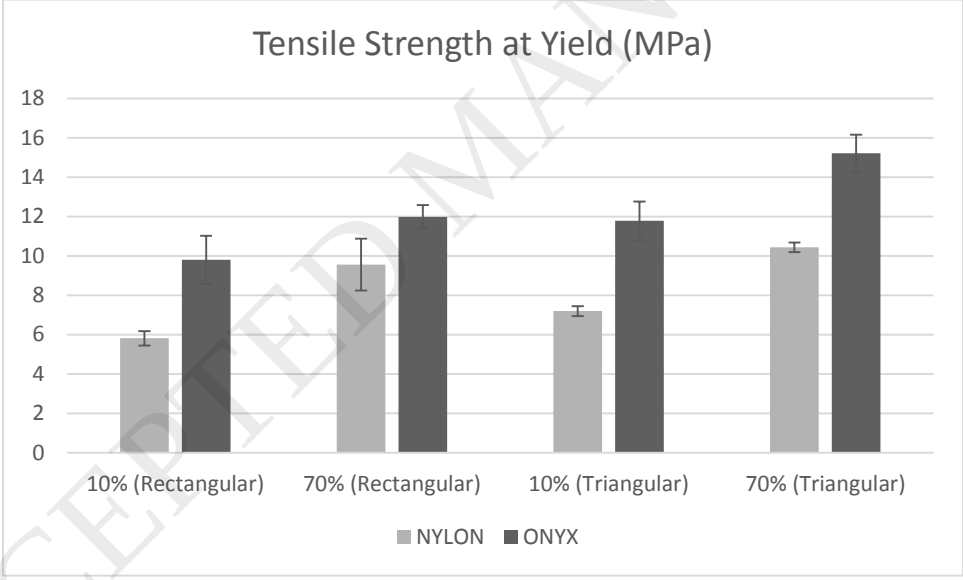

Figure 6. Effect of densities and infill patterns on the Tensile Strength at Yield of Nylon and Onyx.

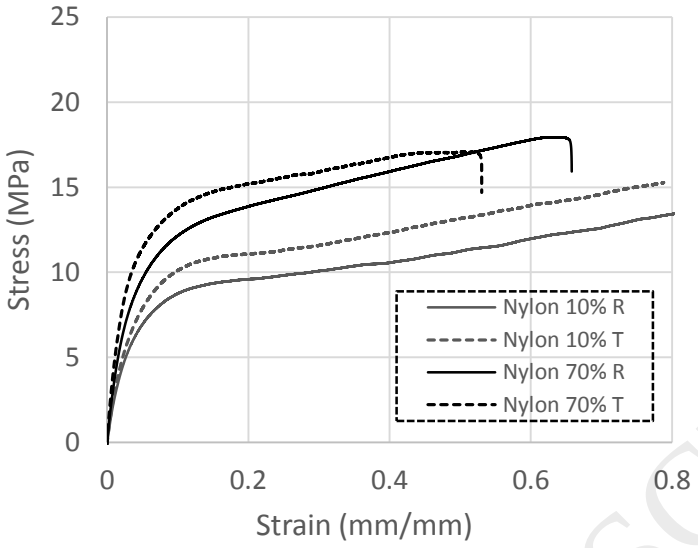

a)

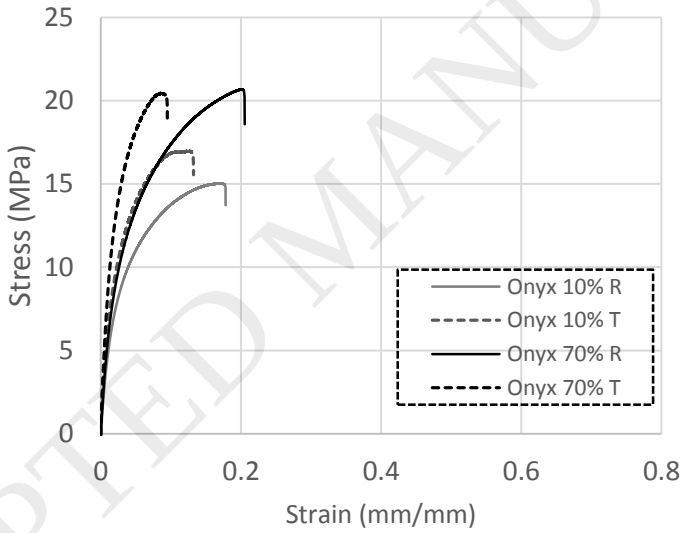

b)

Figure 7: Stress-Strain Curves Experimental Setup 1a) Nylon samples b) Onyx samples.

The data obtained in Experimental Setup 1 was analyzed in Minitab 17 through an Analysis of Variance (ANOVA). Results suggest that the differences between the means of the different materials are statistically significant for the elastic modulus and tensile strength in the three factors analyzed. The ANOVA study was conducted with a confidence level of 95% and a significance level of α=0.05. The significance (p-values less than 0.05) of raw material (Onyx vs. Nylon), infill density (10% and 70%) and infill patterns (Rectangular and Triangular) were proved in all cases. Figure 8 presents the Pareto charts of the standardized effects for Experimental Setup 1, in support of the previous statements. Similarly, Appendix 2 shows the summary of results from ANOVA analysis.

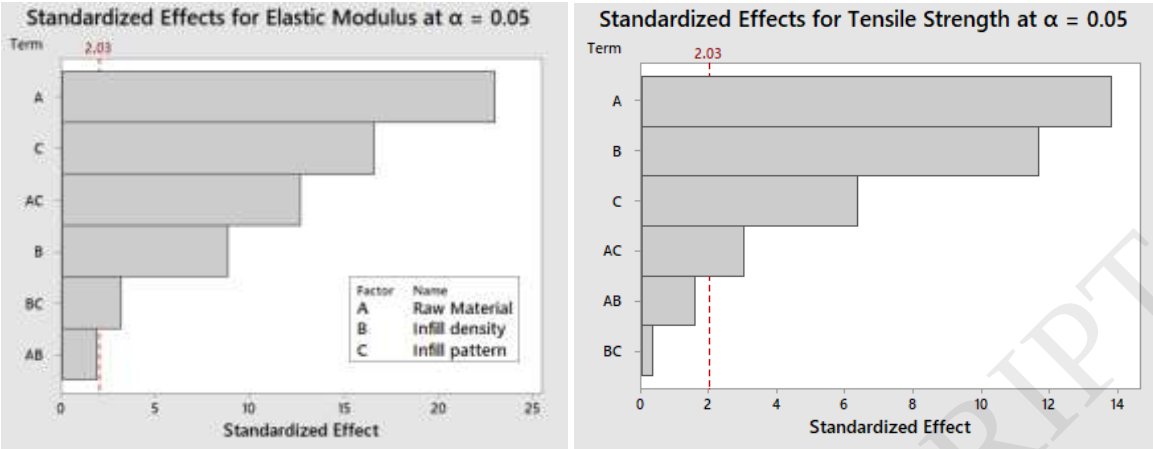

Figure 8. Pareto charts with the significance effects of Experimental Setup 1.

4.2.2. Discussion

The results from ANOVA analysis indicate that the elastic modulus for the two materials are definitely different (Factor A). For both materials on the Elastic Modulus, the analysis shows that infill pattern (Factor C) had a more important effect than infill density (Factor B). Regarding the tensile strength, the materials again have different values (Factor A). However, the study shows that the infill density (Factor B) has a higher effect than the infill pattern on strength. For the interaction between factors, raw material-infill pattern (AC) and infill density-infill pattern (BC) affect elastic modulus, while only raw material-infill pattern (AC) is statistically significant for tensile strength.

The Analysis of Variance is consistent with the values of tensile properties presented in Figures 5 and 6, where the infill pattern has a considerable effect on the mechanical properties. In particular, the Onyx specimens with a triangular pattern show an increment of ~80-105% for elastic modulus, and ~20-25% more for tensile strength compared with the rectangular pattern samples; while the Nylon specimens with a triangular pattern show an increment of 15-22% for elastic modulus, and ~9-24% more for tensile strength compared with the rectangular pattern samples.

The values obtained in Setup 1 are lower than the values found in Markforged datasheets [22]. This is likely due to the fact that the specimens in Setup 1 have much less infill than Markforged samples, and a different geometry (ASTM D638 Type IV) was tested for datasheet. As a verification experiment, a Nylon specimen with 100% of infill density and Triangular pattern was fabricated and tested. The specimen shows an elastic modulus of 945.9 MPa similar to Markforged datasheet (940 MPa) and reach a tensile stress at break of 34 MPa.

4.3. Tensile Results Experimental Setup 2: Continuous Carbon Fiber Reinforced Composites

Figures 9 and 10 show the effects of printing architecture and volume fraction on the tensile properties of the specimen for continuous carbon fiber reinforcement samples.

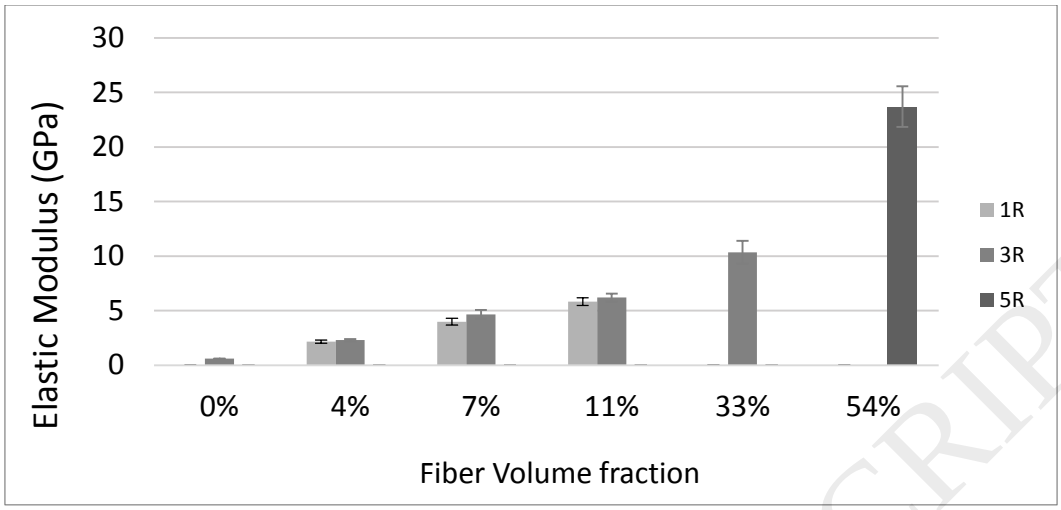

Figure 9. Effects of Fiber Volume Fraction and Printing architecture (1R, 3R and 5R) on Elastic Modulus.

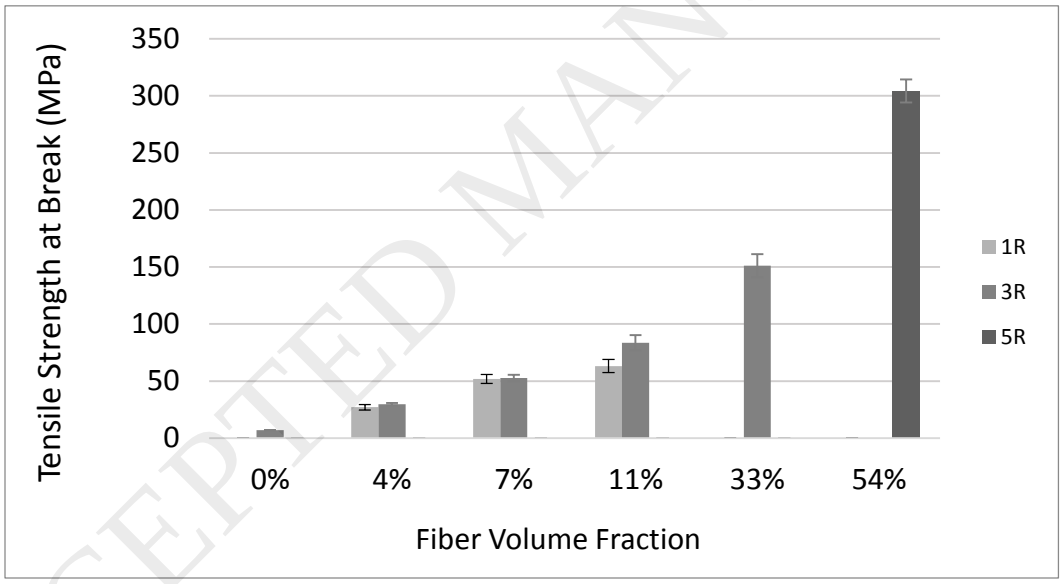

Figure 10. Effects of Fiber Volume Fraction and Printing architecture (1R, 3R and 5R) on Tensile Strength.

The tensile properties obtained for continuous carbon fiber reinforced composites proved to be significantly better than the rest of the specimens in Setup 1. The increase in the elastic modulus can go up to 25 times E_{nylon} (Nylon 100% Triangular) reaching 23.7 GPa for 5R-18L test, which is close to E for commercial Fiber-glass (25 GPa) or Kevlar (25 GPa) composites; although it is only one third of the E reported for standard Carbon Fiber composites (70 GPa) [30]. The tensile strength of 5R-18 L samples reached 304.28 MPa, which is close to TS = 310 MPa reported for Aluminum 6061-T6. [31]. Similar performance was reported by Dickson et al. [6], who presented composite specimens with yield strengths

of up to 368 MPa with volume fraction of 35% carbon fiber. Figure 11 shows the Stress-Strain curves, while Figure 12 present the Pareto charts of the standardized effects for Experimental Setup 2. Appendix 3 shows the summary of results from ANOVA analysis.

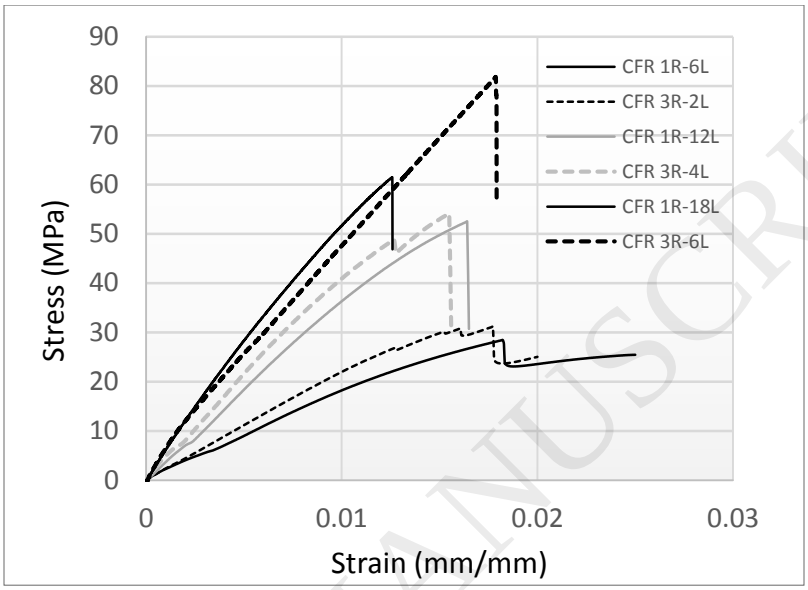

Figure 11. Stress-Strain Curves Experimental Setup 2.

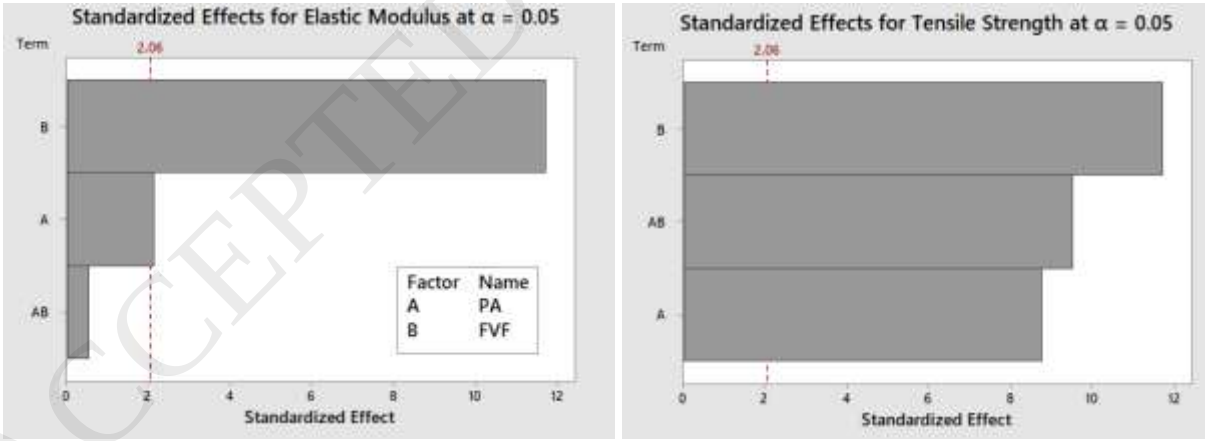

Figure 12. Pareto charts with the significance effects of Experimental Setup 2.

The data in Setup 2 was also analyzed in Minitab 17 through an ANOVA. Results suggest that the differences between the means are statistically significant (p-values less than 0.05) for the two factors: Fiber Volume Fraction and Printing Architecture. A comparison of the two printing architectures (3R compared with 3 times of 1R) with the same volume fraction, suggests that the arrangement of fibers affects tensile properties, with a better performance for wider arrangement (3R). FDM is a layer by layer process. When

3R samples are manufactured, the fiber rings are printed in the same pass. Figure 13a shows a magnified image of a 3R sample. On the other hand, 1R rings are printed in different layers. Figure 13b shows magnified images of the cross section of a 1R sample. In Figure 13c non-uniform wetting of the fibers bundles by the matrix can be observed . Differences in thermal patterns or pressure of deposition of these proceses may have an effect on the properites of the samples. A definite explanation for this behavior requires further study, however.

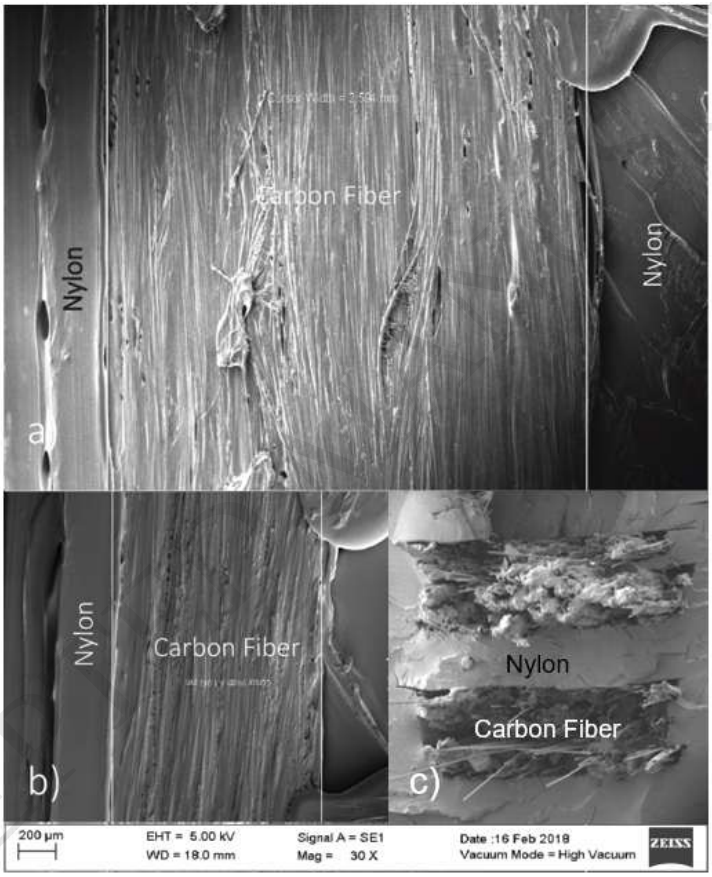

Figure 13. a) 3R layer top view b) 1R layer top view c) 1R cross-section view.

4.4. Meso-structure analysis Experimental Setup 1 and 2

Specimens were 3D printed with Onyx and their fabrication was stopped at the middle (Layer 13). These samples were observed with a Stereo ZEIS optical microscope to have a better understanding of how the infill patterns are constructed. Two infill patterns (Rectangular and Triangular) and two infill densities (10% and 70%) were analyzed and their angles were measured. Good correspondence with the theoretical orientation angles of 45° for a rectangular shape and 0°/60° for triangular shape was found. However, the "density" of strands between the two patterns types shows significant differences, as seen in Figure 14. The

rectangular shape appears to have a higher infill density. This is because the strands are printed alternately at + /- 45° with respect to the tension axis. Under these conditions, the contact area between the strands is reduced, while in the triangular shape all the strands are stacked in the same orientation.

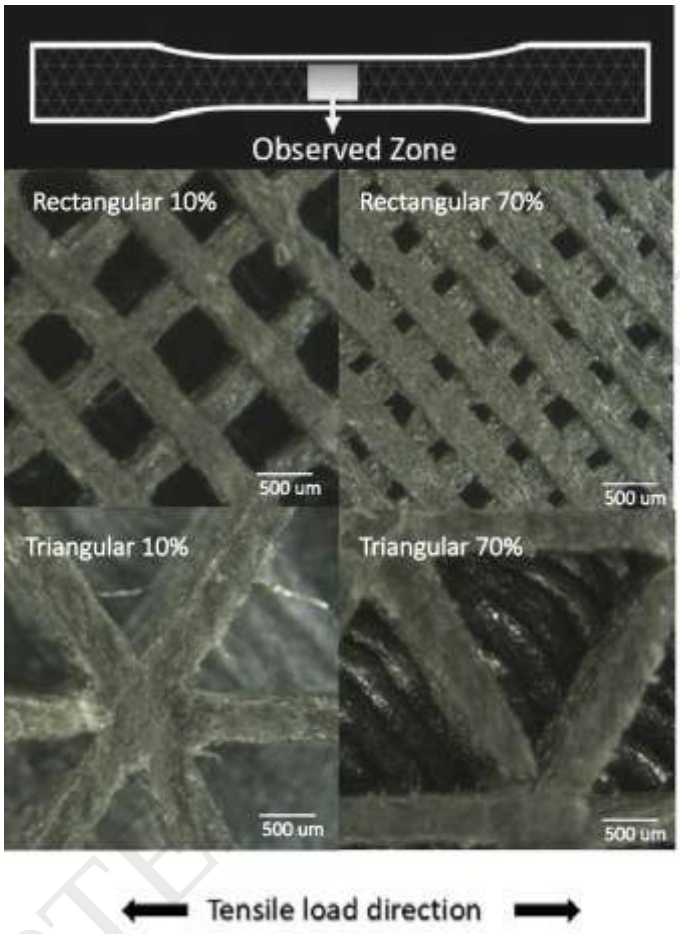

Figure 14. Infill Geometries (Rectangular & Triangular) and Densities (10% & 70%) tested in Onyx samples.

For all the tests in Experimental Setup 1, Nylon and Onyx specimens, the Triangular shape (T 0°/60°) has a better tensile performance because there are more strands that are oriented at 0° (in the direction of the load). The better contact and the orientation of the stacked strands provides a better mechanical performance. Figure 15 shows the arrangement of strands in triangular and rectangular patterns.

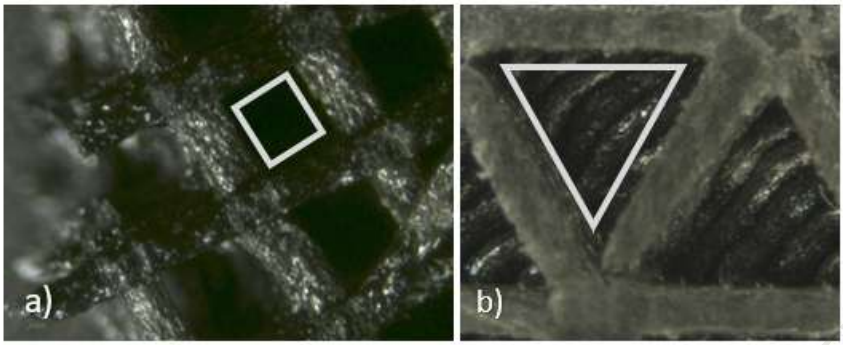

Figure 15. Arrangement of printing strands at a) Rectangular pattern b) Triangular Pattern.

For CFR composites, the mechanical properties increased considerably by increasing volume fraction of the reinforcement fiber. Individual diameters of the reinforcement fiber of a broken sample were measured using an SEM EVO MA25 ZEISS microscope. The software reported the following fiber diameters: 6.98 μm, 8.816 μm, 7.939 μm and 7.254 μm. These values are in the low end of the advertised data (10 ±2 μm), and some fall out if this range. The broken carbon fibers are shown in Figure 16. Again, it can be seen that the individual fibers do not appear to be wetted well by the matrix.

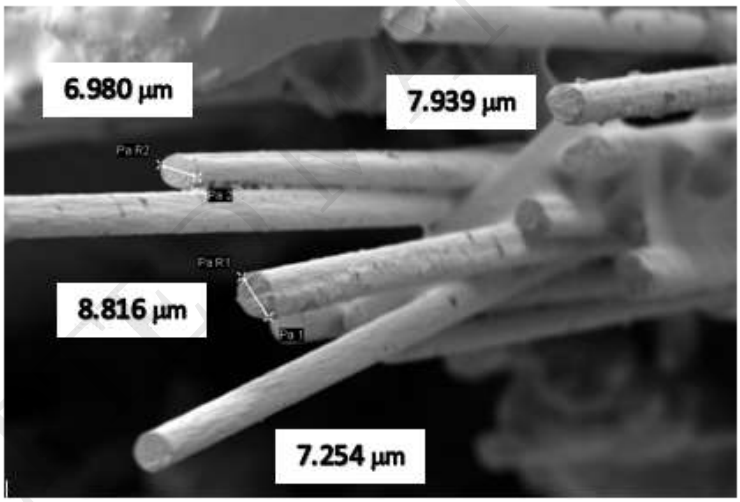

Figure 16. Carbon fibers measurements after fracture.

4.5. Fracture Mechanism analysis Experimental Setup 1 and 2

As shown in several studies [32] [33] [34] [35] [36], the integrity and mechanical properties of AM parts are directly related to the mesostructure of fused filament fabricated parts, *i.e*. the void geometry and the bonding between individual polymer strands. Since infill density is below 100% in all samples, mechanical properties are determined predominantly by the individual strands.

When the fracture mechanisms of the Nylon and Onyx samples are compared, it can be seen that the Nylon samples fail in a macroscopically ductile manner, while Onyx displays a macroscopically more brittle failure. Nylon samples show an initial visco-elastic behavior up to a macroscopic engineering strain

of ±0.15 (see Figure 17), *i.e.* the yield point. As one of the strands exceeds this yield point, it exhibits microscopically plastic strain localization and does not contribute any more to the overall force the sample can endure. As a consequence, the effective area is reduced, and neighboring strands also reach their yield stress, until the whole sample exhibits macroscopically plastic strain flow. This is manifested by a stress that stays almost constant (up to an engineering strain of ±0.25). The material then starts to strain harden and, as a consequence, the stress is increasing again. In this region, the sample rapidly starts to elongate until macroscopic final failure, when the maximum tensile stress is reached across the whole sample cross-section. This failure mechanism is shown in Figure 18a, where elongated strands can be detected and a deformed shape of the initially rectangular geometry can be seen.

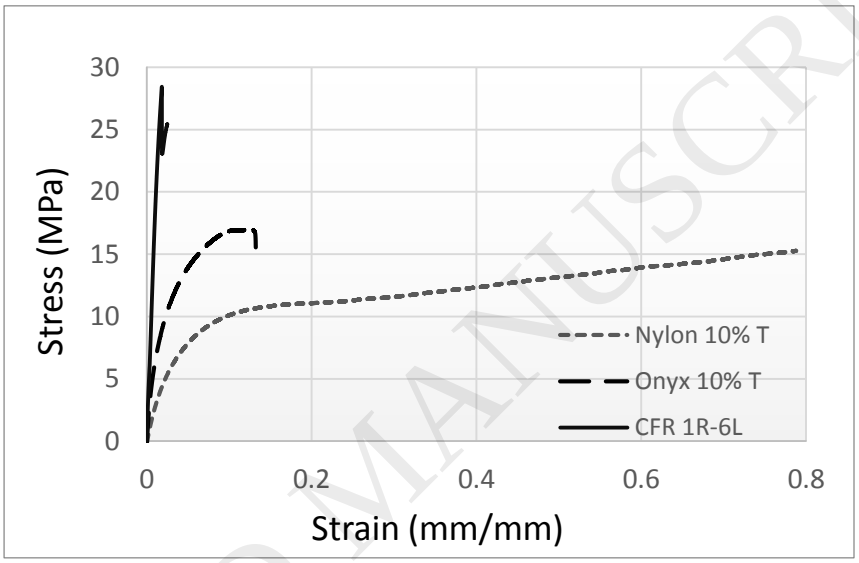

Figure 17. Mechanical behavior curves Nylon, Chopped composites (Onyx), and CFR composites

The Onyx failure mechanism is somewhat different. Due to the chopped carbon fibers which are supported by a Nylon matrix, the material has an increased elastic modulus and breaks right after reaching the macroscopic ultimate stress, which coincides with the yield point at a macroscopic engineering strain of ±0.10 (see Figure 17). The failure mechanism starts when one of the strands reaches locally its ultimate stress value. However, in this case, the strand immediately breaks, as that stress is above the ultimate tensile stress of the Nylon matrix. This causes a sudden increased stress concentration in the neighboring strands and their subsequent failure. An overall *macroscopic* brittle failure is the result, as is shown in Figure 17. Figure 18b shows this brittle failure mechanism in a surface layer of an Onyx sample, where no extended Nylon ligaments can be detected.

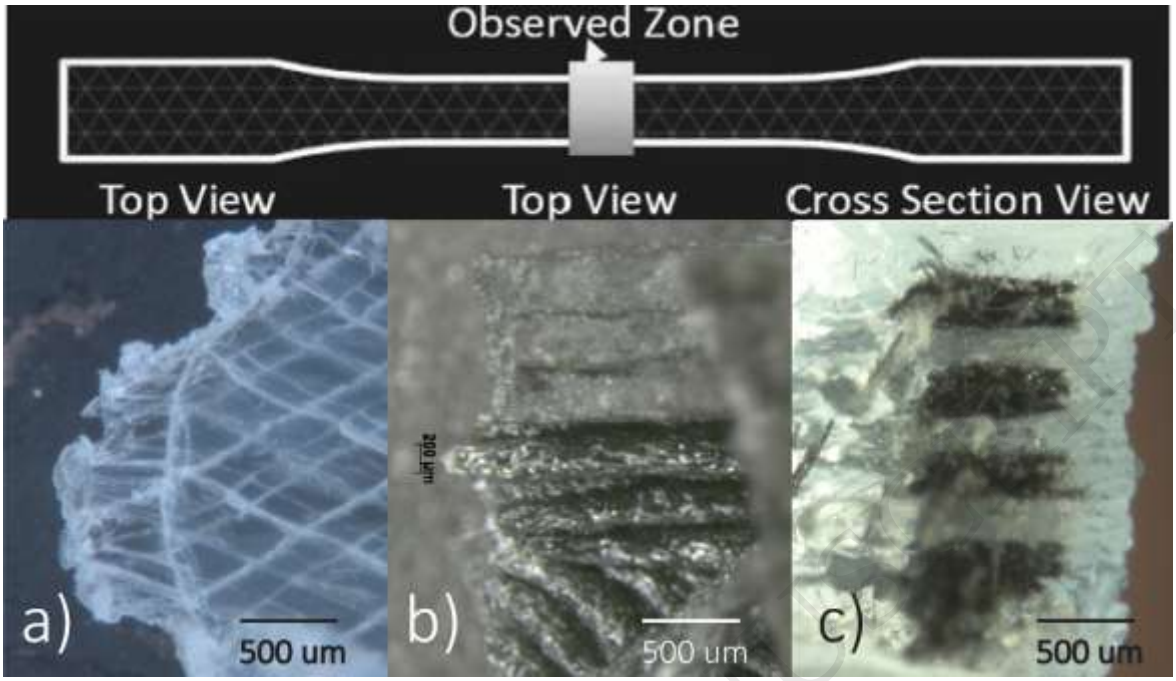

Figure 18. Close-up view of failure mechanism of a) Nylon specimen; b) Onyx sample c) CFR specimen.

The failure mechanism of the CFR samples is rather similar to the Onyx samples, also showing macroscopically brittle failure. The continuous bundles of carbon fibers are responsible for withstanding the forces applied to the samples, with a high elastic modulus and a limited maximum elongation (see Figure 17). At the moment these fiber bundles reach their maximum stress, they break and cause a sudden increase in the stress of the neighboring Nylon strands, far above the stresses these Nylon strands can withstand. These then exhibit a very limited local plastic strain flow, resulting in a macroscopically brittle failure behavior, as shown by the stress-strain curve. An image of a broken carbon fiber bundle and its neighboring Nylon strand with limited plastic strain flow, *i.e.* elongated Nylon ligaments, is shown in Figure 18c.

5. Comparison of Elastic Modulus: experimental values vs estimation by a geometric approach of Rule of Mixtures

For the prediction of elastic modulus of for CFR composites, Melenka et al. [14] proposed a Volume Average Stiffness (VAS) Method. The VAS involves three main steps. First, micromechanical models are used to determine the elastic constants for each of the four regions (shown in Section 4.1). Once the micromechanical properties of the roof / floor, infill and walls regions are determined, the compliance matrices for a transversely isotropic material can be populated. Third, the stiffness averaging is performed by establishing the volume fraction of each section within the test specimen in order to determine the contribution of each section to the overall mechanical properties. Finally, to determine the effective mechanical properties of the fiber reinforced 3D printed parts the global stiffness matrix is inverted, and the effective elastic constants can be obtained.

Following the method by Melenka, a simplified approach to predict the elastic modulus based on the Rule of Mixtures (ROM) is presented here. The contribution of the roof / floor, infill and walls regions is calculated by Equation 7, that calculates the volume fraction of the matrix (φ_{matrix}). For the presented approach the elastic modulus of the composite can be obtained from Equation 8, by reducing the compliance matrix to only one constant, assuming the specimen behaves in an isotropic manner.

$$\varphi_{matrix} = \frac{V_{\text{roof and floor}} + V_{wall} + V_{infill}}{V_{composite}} \quad (7)$$

$$Rule\ of\ mixtures\ composites:\ E_{predicted} = \varphi_{matrix} E_{matrix} + \varphi_{fiber} E_{fiber} \quad (8)$$

Predicted values of elastic moduli were calculated using the values described in Table 4 and the elastic modulus of raw materials values of $E_{matrix} = 940\ MPa$ and $E_{cf} = 50\ GPa$ obtained from Markforged materials datasheet [37]. Predicted values were compared to experimental data. Results are summarized in Table 4.

Table 4. Results from Prediction Model by Rule of Mixtures

Printing Architecture	Matrix Volume Fraction	Fiber Volume Fraction	Elastic Modulus (MPa)		Error
			Measured	Predicted	
1R-6L	44.8%	4%	2152.0	2224.1	3%
3R-2L	46.2%		2295.4	2236.7	-3%
1R-12L	42.8%	7%	3988.9	4008.0	0%
3R-4L	45.5%		4471.4	4033.3	-10%
1R-18L	40.8%	11%	5830.2	5791.9	-1%
3R-6L	44.8%		6197.4	5829.3	-6%
3R-18L	40.8%	33%	10348.6	16609.2	60%
5R-18L	40.8%	54%	23690.6	27426.5	16%

A good agreement between measured and predicted values was found for the tests with volume fraction lower than 11%. However, for the fractions higher than 11% the rule of mixture was less accurate. This behavior is consistent with the values reported by Van Der Klift et al. [15] who also found that at higher volume fractions this kind of composite does not behave according to the rule of mixtures. In contrast, Melenka´s method shows good correlation for larger amount of fiber reinforcement. However, for lower fiber reinforced contents, the method fails to predict the elastic modulus.

The difference of the approach presented here with respect to Melenka´s method is that the micro-mechanics model does not consider the anisotropic nature of the fiber. The compliance matrix is reduced to a single constant E. The proposed method provides a simple way to estimate the expected mechanical performance of CFR composites with lower fiber contents, where the mechanical behavior of the composite is dominated by the matrix (Nylon). For a larger amount of fiber, the composite must be treated as a transversely isotropic material and Melenka´s method is more effective to predict the elastic constants. This behavior should be expected for CFR printed parts, because the integrity of the fiber / matrix interface may affect the efficiency of load transfer. As can be seen in Figures 13c (and Figure 22c), voids may be found between Nylon strands and fiber bundles.

6. Results and Discussion for Setup 3

6.1. Starting point location

In Experimental Setup 2, most of the specimens fractured in the same area close to the inflection point in the dog bone. Previous studies by Dickson et al. [6] suggested that the crack initiation coincides with this region due to shear forces experienced by the change in fiber alignment, and through FEM simulation demonstrated the locations of the highest third major stresses (regions of highest compression) in these points. In contrast, Melenka et al. [14] argued that the break occurs at the starting point of fiber reinforcement.

As explained before, a third experimental setup was conducted to analyze the effect of moving the initial point of reinforcement deposit. The goal was to analyze the phenomena that produce the failure in the CFR samples. Figure 19 shows the printed samples and the differences in the start point of fiber reinforcement. Figure 19a shows the configuration used for all the previous tests, with a start point outside the tensile area. For most applications, it is not always possible to keep the starting point of reinforcement outside the load area. The effects of the location of the initial point of reinforcement inside the tensile area were evaluated with two tests: Middle (Figure 19b) and Distributed (Figure 19c).

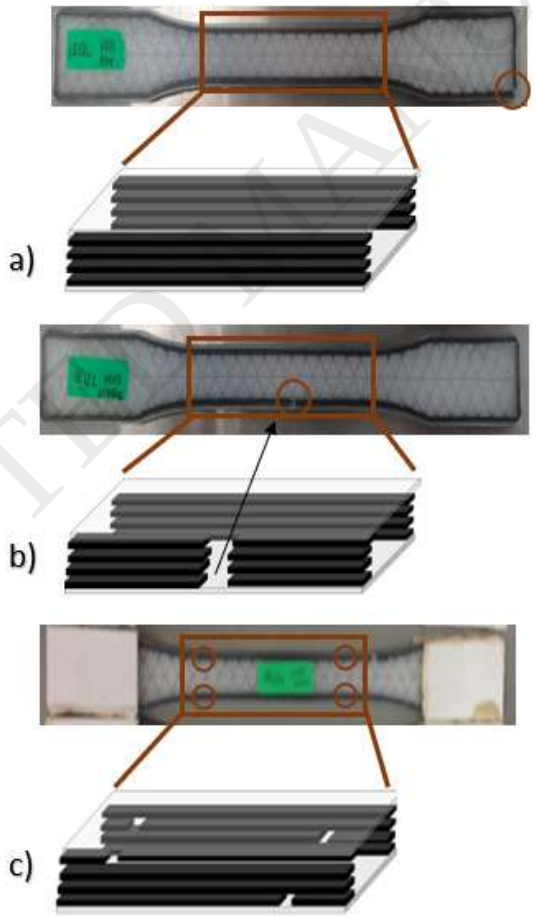

Figure 19. Specimens and schematics of 1R-12L with different start points at a) Outside (Tip), b) Middle c) Distributed over the tensile area. (Fiber starting point locations are shown in circles.)

6.2. Tensile Test Results Experimental Setup 3: Effect of initial point of reinforcement

Table 5 summarizes the values for elastic modulus and the tensile strength of the Middle and Distributed tests and compared with the regular test (Outside). Figure 21 shows the stress-strain curves for the different specimens tested.

Table 5. Results from Tensile Test (ASTM D638) for Experimental Setup 3.

		Elastic Modulus (MPa)		Tensile Strength (MPa)	
Fiber Arrangement	Fiber Reinforced start point	Mean	St. Dev.	Mean	St. Dev.
1R-12L	Distributed	4325.7	79.5	57.7	3.4
	Outside	3988.9	311.2	51.8	3.9
	Middle	3314.7	193.4	43.3	2.6

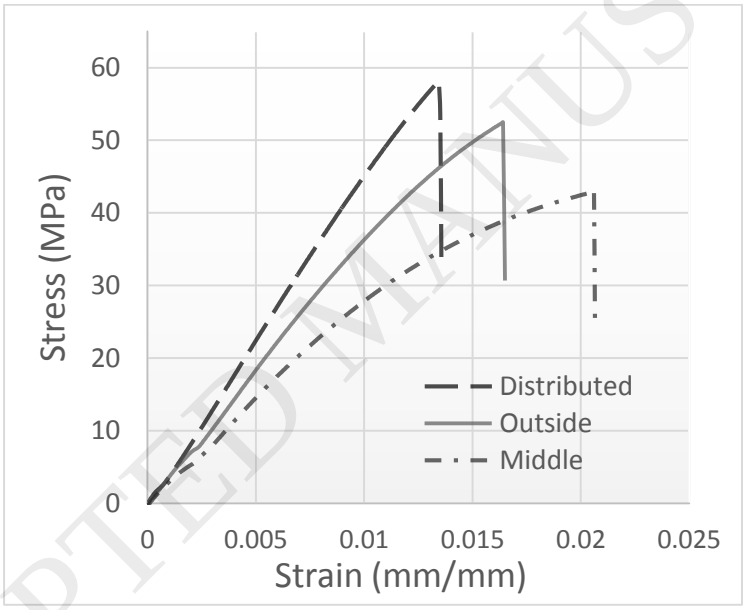

Figure 20. Stress-Strain Curves Experimental Setup 3.

The middle samples of 1R 12L compared with the Outside test exhibit a decrease of 16.9% in the elastic modulus and 16.5% in the tensile strength. To overcome this limitation, the test with distributed start points over the tensile area was proposed. The Distributed test shows good tensile results. The samples exhibit an increase of 8.4% in the elastic modulus and 11.3% in the tensile strength compared to Outside test. This is probably due to the distribution of the start points, which releases some compression stresses in the inflection area, preventing the crack initiation in the first fracture mechanism (Figure 21), while the stacked distribution creates only small defects that are not critical for the second mechanism (Figure 22), described in the next section.

6.3. Fracture Mechanism analysis Experimental Setup 3

A SEM inspection of the 1R-12L samples in experimental Setup 3 suggests that fracture is different for the samples where the starting point of deposition of the fiber reinforcement is outside the tensile area (in the regular test, refered to as "Outside" in previous sections), compared with samples where the starting point is in the middle of the tensile area (denominated "Middle") or distributed over different points within the tensile area (denominated "Distributed"). These different starting points influence the mechanical properties, such as the elastic modulus and ultimate tensile strength. Therefore, the fiber reinforcement starting point should be considered as a critical design parameter.

Figure 21 shows details about the fracture mechanism when the start of reinforcement is outside the tensile area. Figure 21a shows a cross-section zone where both carbon fibers and Nylon strands are present and visible. It can be seen that fracture has started at the fiber bundles, with brittle fiber bundle failure and a certain amount of fiber pull-out. In Figure 21b, some of the carbon fibers affected by fiber pull-out are shown, with a brittle failure surface. Figure 21c shows an image of a cross-section zone with only Nylon strands, also demonstrating a brittle failure surface and very limited local plastic strain flow *i.e.* in the form of elongated Nylon ligaments.

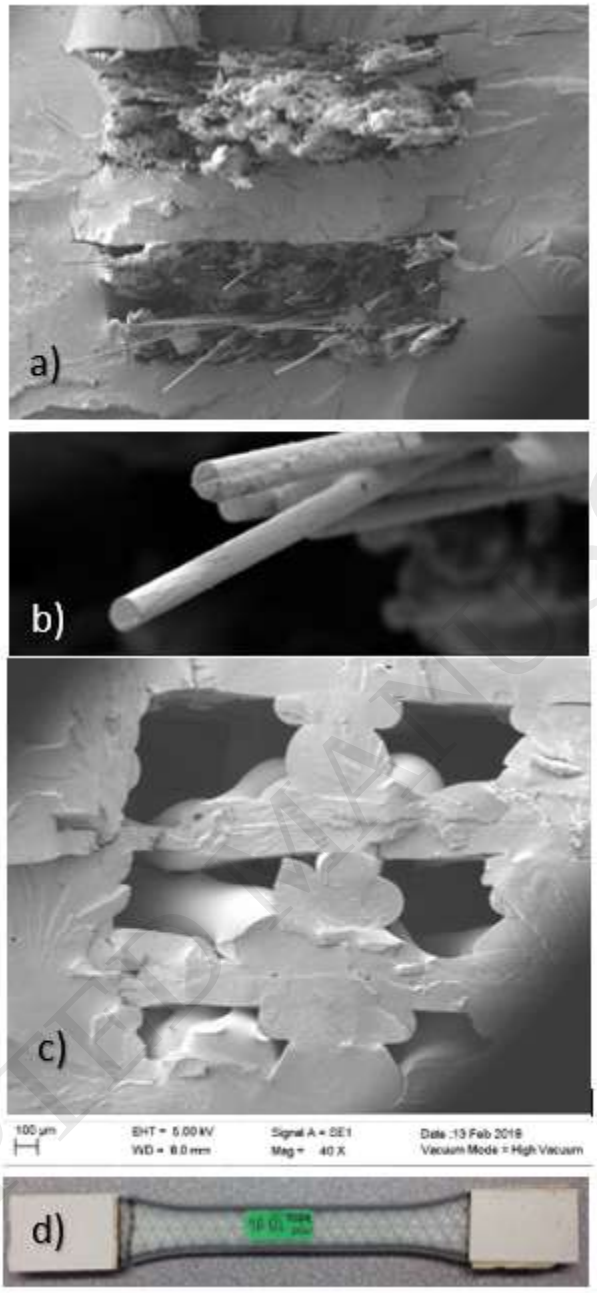

Figure 21. Fracture mechanism for fiber start outside the tensile area (denominated "Outside"). a) Continuous fiber-reinforced section, b) Single carbon fiber fracture, c) Nylon area section d) Fractured specimen.

Figure 22 shows images of a specimen where the starting point of the fiber reinforcement is in the middle of the tensile area. Failure occurs at the cross-section where the starting point of the deposit of reinforced fibers is present, see Figure 22d. In that particular cross-section, there is a small zone with no fiber bundles present (see Figure 22d, side of start point). Since there are less fiber bundles present to withstand the tensile force, this results in a lower macroscopic ultimate tensile stress. From Figure 22a, a right-hand microscope view of the break surface area on the side of the start point, it can be seen that the

carbon fiber bundles on this side of the tensile sample do not contribute to the ultimate tensile force, as no fiber failure nor fiber pull-out is detected. At the side of the starting point, in the zone of the cross-section where only Nylon strands are present, the Nylon strands can undergo more pronounced *local* plastic strain flow, as can be seen in Figure 22b where some extended Nylon ligaments can be detected. Once the ultimate tensile force of the fiber bundles is reached, the cross-section fails in a similar manner as for the previous "Outside" case, *i.e.* brittle fiber bundle failure and a certain amount of fiber pull-out; compare Figure 21a and Figure 22c

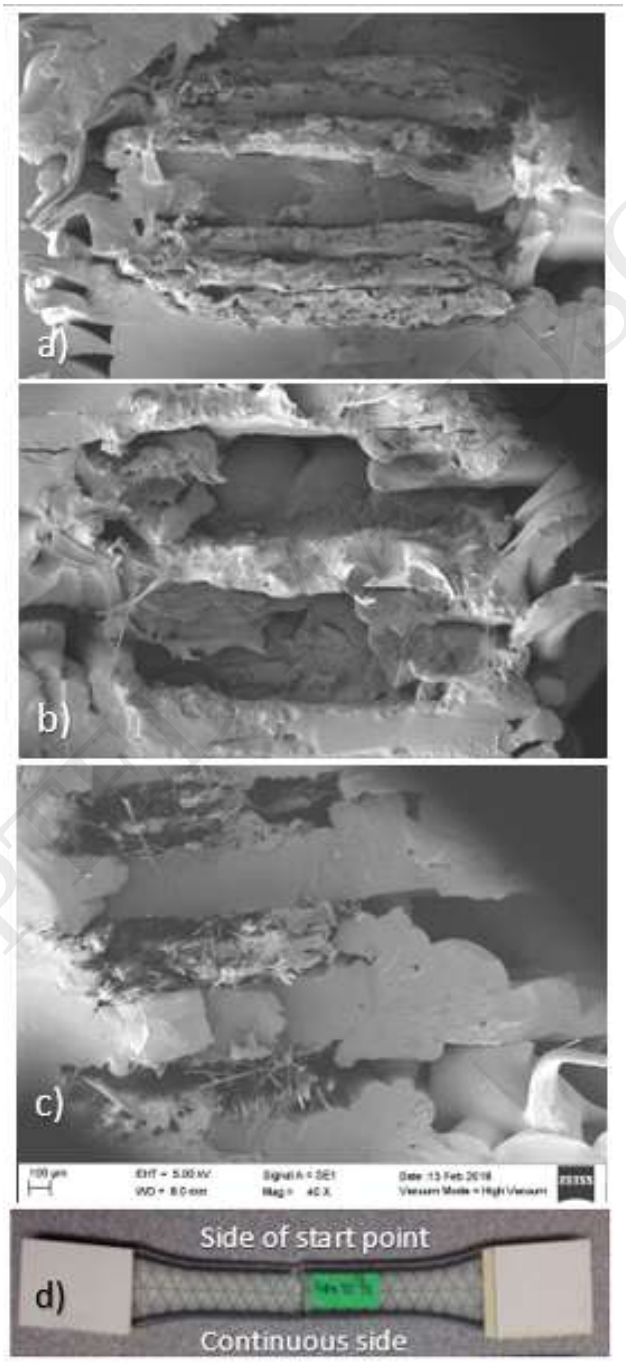

Figure 22. Fracture mechanism for fiber start inside the tensile area ("Middle") a) Side of starting point (right view with carbon fiber bundles) b) Opposite Side of starting point (left view, only Nylon strands,

without carbon fiber bundles) c) Continuous fiber-reinforced side d) Fractured specimen.

7. Implications for Part Design

Based on the previous results, and to make better use of the capabilities of the process for 3D printed composites, designers should consider the following recommendations:

- Use the triangular infill pattern, especially for chopped composites.
- The infill density (the amount of matrix material deposited inside the part) has a minor role in the tensile properties. Reducing the infill density results in lower printing costs and should be seen as an option, if conditions allow. For example, Onyx Rectangular samples with 70% of infill density take 69 min to print, while 10% samples take 48 min. Thus, strength is reduced by 7.4% while cycle time is reduced by 30.4%.
- Use a wider arrangement of the fiber reinforced strands, instead of stacked strands of fiber reinforcement.
- The designer must consider the fracture mechanisms discussed in Section 6.3. Avoid placing all the initial points of fiber in a single place. Fixing the initial points of fiber in a distributed manner helps improve overall part strength.

Clearly, these recommendations are based on the study of standard specimens. The effect on real parts needs to be assessed in future studies.

8. Conclusions and Future Work

8.1. Conclusions

In this work, 3D printed composites with continuous carbon fiber reinforcement and chopped carbon fiber (Onyx) composites were manufactured and tested. Onyx samples show small improvements with respect to Nylon. Results showed that factors such as infill density and infill patterns in 3D printed chopped composites affect part strength. As discussed, the Triangular shape has a better tensile performance and should be used whenever possible.

The influence of fiber volume fraction (VF) and fiber placement arrangement on continuous carbon fiber reinforcement composites were measured. As expected, the tensile properties for CFR composites have much better performance when the amount of fiber is increased. From the comparison of the two printing architectures (1R vs 3R) with the same volume fraction, it was shown that the arrangement of fibers has an effect on tensile properties with a slightly better performance for the wider arrangement. The effects of moving the initial point of reinforcement deposit on the fracture mechanisms, elastic moduli and tensile strength were also studied.

A variation of the ROM method to predict elastic modulus for CFR composites with lower fiber content that considers different geometric characteristics was proposed. Good correspondence between predicted and experimental data was found for volume fractions smaller than 11%.

Findings may help the designer to define the best parameters for the print part, and should also be helpful for the design of 3D printed composites.

8.2. Future Work

There are three directions for future work. First, as explained in Section 4.2, the behavior of the 3R vs 1R requires further study. The AM machine will be supplied with instrumentation to measure changes in thermal patterns in the specimens during processing. Second, Computer Tomography (CT) will be used to observe fiber behavior of 3D printed carbon fiber and fiberglass composites under uniaxial tension. The goal would be to measure and observe irregularities, such as first fiber strands broken, void areas or non-uniform distribution of the thickness strands. Of particular interest is to determine the "load elastic limit", when the first critical defects appear in this kind of composite specimens. Finally, the effect of the use of design recommendations on real parts needs to be assessed in test cases.

Declaration of conflicting interests

The author(s) declared no potential conflicts of interest with respect to the research, authorship, and/or publication of this article.

Acknowledgments

This work was funded by the Automotive Consortium for Cyber-Physical Systems research group at Tecnológico de Monterrey. Graduate student's economic support was provided by CONACyT (Consejo Nacional de Ciencia y Tecnologia). The support of the laboratory facilities was provided by the Structural Integrity Research Group, University of Burgos and Centro de Innovación en Diseño y Tecnología (CIDyT), Tecnologico de Monterrey

References

[1] F. Ning, W. Cong, Y. Hu, and H. Wang, "Additive manufacturing of carbon fiber-reinforced plastic composites using fused deposition modeling: Effects of process parameters on tensile properties," *J. Compos. Mater.*, vol. 51(4), pp. 451–462, 2016.

[2] K. V. Wong and A. Hernandez, "A Review of Additive Manufacturing," *ISRN Mech. Eng.*, vol. 2012, pp. 1–10, 2012.

[3] X. Wang, M. Jiang, Z. Zhou, J. Gou, and D. Hui, "3D printing of polymer matrix composites: A review and prospective," *Compos. Part B Eng.*, vol. 110, pp. 442–458, 2017.

[4] G. T. Mark, "Apparatus for Fiber Reinforced Additive Manufacturing Pub. No.: US 2014/0328963 A1," 2013.

[5] F. Baumann, J. Scholz, and J. Fleischer, "Investigation of a New Approach for Additively Manufactured Continuous Fiber-reinforced Polymers," *Procedia CIRP*, vol. 66, pp. 323–328, 2017.

[6] A. N. Dickson, J. N. Barry, K. A. McDonnell, and D. P. Dowling, "Fabrication of continuous carbon, glass and Kevlar fibre reinforced polymer composites using additive manufacturing," *Addit. Manuf.*, vol. 16, pp. 146–152, 2017.

[7] I. Daniel, I. M., Ishai, O., Daniel, I. M., & Daniel, *Engineering mechanics of composite materials*, Second. Oxford University Press, 2006.

[8] H. Prüß and T. Vietor, "Design for Fiber-Reinforced Additive Manufacturing," *J. Mech. Des.*, vol. 137, no. 11, p. 111409, 2015.

[9] Stratasys, "FDM Nylon 12CF Datasheet," 2018. [Online]. Available: http://www.stratasys.com/es-mx/nylon12cf. [Accessed: 05-Apr-2018].

[10] C. Yang, X. Tian, T. Liu, Y. Cao, and D. Li, "3D printing for continuous fiber reinforced thermoplastic composites: mechanism and performance," *Rapid Prototyp. J.*, vol. 23, no. 1, pp.

209–215, 2017.
[11] X. Tian, T. Liu, C. Yang, Q. Wang, and D. Li, “Interface and performance of 3D printed continuous carbon fiber reinforced PLA composites,” *Compos. Part A Appl. Sci. Manuf.*, vol. 88, pp. 198–205, 2016.
[12] M. Eichenhofer, J. C. H. Wong, and P. Ermanni, “Continuous lattice fabrication of ultra-lightweight composite structures,” *Addit. Manuf.*, vol. 18, pp. 48–57, 2017.
[13] M. Eichenhofer, J. C. H. Wong, and P. Ermanni, “Exploiting cyclic softening in continuous lattice fabrication for the additive manufacturing of high performance fi bre-reinforced thermoplastic composite materials,” *Compos. Sci. Technol.*, vol. 164, no. March, pp. 248–259, 2018.
[14] G. W. Melenka, B. K. O. Cheung, J. S. Schofield, M. R. Dawson, and J. P. Carey, “Evaluation and prediction of the tensile properties of continuous fiber-reinforced 3D printed structures,” *Compos. Struct.*, vol. 153, pp. 866–875, 2016.
[15] F. Van Der Klift, Y. Koga, A. Todoroki, M. Ueda, Y. Hirano, and R. Matsuzaki, “3D Printing of Continuous Carbon Fibre Reinforced Thermo-Plastic (CFRTP) Tensile Test Specimens,” *Open J. Compos. Mater.*, vol. 6, no. 1, pp. 18–27, 2016.
[16] S. Christ, M. Schnabel, E. Vorndran, J. J. Groll, and U. Gbureck, “Fiber reinforcement during 3D printing,” *Mater. Lett.*, vol. 139, pp. 165–168, 2015.
[17] D. Türk, L. Triebe, and M. Meboldt, “Combining Additive Manufacturing with Advanced Composites for Highly Integrated Robotic Structures,” *Procedia CIRP*, vol. 50, pp. 402–407, 2016.
[18] A. Ebn, M. Zogg, and I. Ag, “Additive Manufacturing of Structural Cores and Washout Tooling for Autoclave Curing of Hybrid Composite Structures,” *J. Manuf. Sci. Eng.*, vol. 140, pp. 1–14, 2018.
[19] C. C. Spackman, C. R. Frank, K. C. Picha, and J. Samuel, “3D printing of fiber-reinforced soft composites: Process study and material characterization,” *J. Manuf. Process.*, vol. 23, pp. 296–305, 2016.
[20] M. Fernandez-Vicente, W. Calle, S. Ferrandiz, and A. Conejero, “Effect of Infill Parameters on Tensile Mechanical Behavior in Desktop 3D Printing,” *3D Print. Addit. Manuf.*, vol. 3, no. 3, pp. 183–192, 2016.
[21] C. J. Courter, B., Savane, V., Bi, J., Dev, S., & Hansen, “Finite Element Simulation of the Fused Deposition Modelling Process,” in *Proceedings of the NAFEMS World Congress*, 2017, no. June, p. (pp. 11-14).
[22] C. Klahn, B. Leutenecker, and M. Meboldt, “Design for additive manufacturing - Supporting the substitution of components in series products,” *Procedia CIRP*, vol. 21, pp. 138–143, 2014.
[23] Markforged, “Material Specifications Composites Datasheet,” 2018. [Online]. Available: https://static.markforged.com/markforged_composites_datasheet.pdf. [Accessed: 12-Feb-2018].
[24] G. T. Mark, “Methods for Fiber Reinforced Additive Manufacturing Pub. No.: US 2013/0284069 A1,” 2014.
[25] Adams D. and Adams D. F. (U.S. Federal Aviation Administration), “Tabbing Guide for Composite Test Specimens,” 2002.
[26] F. Ning, W. Cong, J. Qiu, J. Wei, and S. Wang, “Additive manufacturing of carbon fiber reinforced thermoplastic composites using fused deposition modeling,” *Compos. Part B Eng.*, vol. 80, pp. 369–378, 2015.
[27] “Fabrication of continuous carbon, glass and Kevlar fibre reinforced polymer composites using additive manufacturing,” *Addit. Manuf.*, vol. 16, pp. 146–152, Aug. 2017.
[28] J. Justo, L. Távara, L. García-Guzmán, and F. París, “Characterization of 3D printed long fibre reinforced composites,” *Compos. Struct.*, vol. 185, no. November 2017, pp. 537–548, 2017.
[29] G. D. Goh, V. Dikshit, A. P. Nagalingam, G. L. Goh, S. Agarwala, S. L. Sing, J. Wei, and W. Y. Yeong, “Characterization of mechanical properties and fracture mode of additively manufactured carbon fiber and glass fiber reinforced thermoplastics,” *Mater. Des.*, vol. 137, no. October 2017, pp. 79–89, 2018.

[30] ACP Composites, "Mechanical Properties of Carbon Fiber Composite Materials, Fiber / Epoxy resin (120°C Cure)," 2014. [Online]. Available: http://www.acpsales.com/upload/Mechanical-Properties-of-Carbon-Fiber-Composite-Materials.pdf. [Accessed: 29-Oct-2018].
[31] A. M. D. S. Matweb, "Aluminium 6061-T6," *Matweb*, 2000. [Online]. Available: http://asm.matweb.com/search/SpecificMaterial.asp?bassnum=ma6061t6. [Accessed: 15-Nov-2017].
[32] M. K. Agarwala, V. R. Jamalabad, N. A. Langrana, A. Safari, P. J. Whalen, and S. C. Danforth, "Structural quality of parts processed by fused deposition," *Rapid Prototyp. J.*, vol. 2, no. 4, pp. 4–19, 1996.
[33] J. F. Rodriguez, J. P. Thomas, and J. E. Renaud, "Characterization of the mesostructure of fused-deposition acrylonitrile- butadiene- styrene materials," *Rapid Prototyp. J.*, vol. 6, no. 3, pp. 175–186, 2000.
[34] J. F. Rodríguez, J. P. Thomas, and J. E. Renaud, "Mechanical behavior of acrylonitrile butadiene styrene fused deposition materials modeling," *Rapid Prototyp. J.*, vol. 9, no. 4, pp. 219–230, 2003.
[35] Q. Sun, G. M. Rizvi, C. T. Bellehumeur, and P. Gu, "Effect of processing conditions on the bonding quality of FDM polymer filaments," *Rapid Prototyp. J.*, vol. 14, no. 2, pp. 72–80, 2008.
[36] D. Türk, F. Brenni, M. Zogg, and M. Meboldt, "Mechanical characterization of 3D printed polymers for fiber reinforced polymers processing," *Mater. Des.*, vol. 118, pp. 256–265, 2017.
[37] Markforged, "Mechanical properties of continuous fibers," 2016. [Online]. Available: https://bastech.com/wp-content/uploads/2016/05/MF_Mark-Two-3D-Printer-DS-Web.pdf. [Accessed: 15-Nov-2017].

Standard Test Methods

1. ASTM D368 Standard Test Method for Tensile Properties of Plastics, Active Standard ASTM D638-14

Appendix 1: Results from Tensile Test (ASTM D638) Experimental Setup 1 and 2

Average and standard deviations found for elastic modulus and tensile strength for tests studied in Setups 1 and 2.

			Elastic Modulus (MPa)		Tensile Stress (MPa)	
Material	**Infill pattern**	**Infill Density**	**Mean**	**St. Dev.**	**Mean**	**St. Dev.**
Onyx	Rectangular 45°	10%	581.6	86.5	9.8	1.2
		70%	627.3	48.1	12.0	0.6
	Triangular 0°x 60°	10%	1064.9	59.7	11.8	1.0
		70%	1293.9	116.1	15.2	0.9
Nylon	Rectangular 45°	10%	311.6	21.0	5.8	0.4
		70%	490.7	34.5	9.6	1.3
	Triangular 0°x 60°	10%	358.4	31.2	7.2	0.3
		70%	598.9	14.1	10.4	0.2
Carbon Fiber + Nylon Matrix	**Fiber VF**	**Case**	**Mean**	**St. Dev.**	**Mean**	**St. Dev.**
	4%	1R-6L	2152.0	148.4	27.2	2.4
		3R-2L	2295.4	96.8	29.7	1.2
	7%	1R-12L	3988.9	311.2	51.8	3.9
		3R-4L	4471.4	335.5	52.7	2.8
	11%	1R-18L	5830.2	390.2	63.2	5.7
		3R-6L	6197.4	361.8	83.7	6.6
	33%	3R-18L	10348.6	139.3	151.1	10.1
	54%	5R-18L	23690.6	1859.4	304.3	10.2

Appendix 2: ANOVA Experimental Setup 1 performed in Minitab for EM (Elastic Modulus) and TS (Tensile Strength)

Elastic Modulus versus Raw Material, Infill density, Infill pattern
Analysis of Variance

Source	DF	Adj SS	Adj MS	F-Value	P-Value
Model	6	4077822	679637	175.40	0.000
Linear	3	3408812	1136271	293.25	0.000
Raw Material	1	2043216	2043216	527.32	0.000
Infill density	1	301356	301356	77.77	0.000
Infill pattern	1	1064240	1064240	274.66	0.000
2-Way Interactions	3	669010	223003	57.55	0.000
Raw Material*Infill density	1	13115	13115	3.38	0.075
Raw Material*Infill pattern	1	618486	618486	159.62	0.000
Infill density*Infill pattern	1	37409	37409	9.65	0.004
Error	33	127866	3875		
Lack-of-Fit	1	9295	9295	2.51	0.123
Pure Error	32	118571	3705		
Total	39	4205689			

Tensile Strength versus Raw Material, Infill density, Infill pattern
Analysis of Variance

Source	DF	Adj SS	Adj MS	F-Value	P-Value
Model	6	294.252	49.042	63.45	0.000
Linear	3	285.179	95.060	122.98	0.000
Raw Material	1	148.225	148.225	191.77	0.000
Infill density	1	105.625	105.625	136.65	0.000
Infill pattern	1	31.329	31.329	40.53	0.000
2-Way Interactions	3	9.073	3.024	3.91	0.017
Raw Material*Infill density	1	1.936	1.936	2.50	0.123
Raw Material*Infill pattern	1	7.056	7.056	9.13	0.005
Infill density*Infill pattern	1	0.081	0.081	0.10	0.748
Error	33	25.507	0.773		
Lack-of-Fit	1	2.916	2.916	4.13	0.050
Pure Error	32	22.591	0.706		
Total	39	319.759			

Appendix 3: ANOVA Experimental Setup 2 performed in Minitab for EM (Elastic Modulus) and TS (Tensile Strength)

Elastic Modulus versus Printing Architecture, FVF

Factor Information

Factor	Levels	Values
PA	2	1R, 3R
FVF	3	4, 7, 11

Analysis of Variance

Source	DF	Adj SS	Adj MS	F-Value	P-Value
Model	5	77588515	15517703	57.63	0.000
Linear	3	77318767	25772922	95.72	0.000
PA	1	1227819	1227819	4.56	0.043
FVF	2	76090948	38045474	141.30	0.000
2-Way Interactions	2	269748	134874	0.50	0.612
PA*FVF	2	269748	134874	0.50	0.612
Error	24	6462240	269260		
Total	29	84050755			

Tensile Strength versus Printing Architecture, FVF

Factor Information

Factor	Levels	Values
Printing Arch.	2	1R, 3R
FVF	3	4, 7, 11

Analysis of Variance

Source	DF	Adj SS	Adj MS	F-Value	P-Value
Model	5	10114.9	2022.99	154.34	0.000
Linear	3	8698.4	2899.46	221.21	0.000
Printing Arch.	1	1006.2	1006.19	76.76	0.000
FVF	2	7692.2	3846.10	293.43	0.000
2-Way Interactions	2	1416.6	708.28	54.04	0.000
Printing Arch.*FVF	2	1416.6	708.28	54.04	0.000
Error	24	314.6	13.11		
Total	29	10429.5			